Porosity preservation due to grain coating illite/smectite: evidence from Buchan Formation (Upper Devonian) of the Ardmore Field, UK North Sea

Longxun Tang[1]*, Jon Gluyas[1], Stuart Jones[1]

1. Department of Earth Sciences, Durham University, South Road, Durham, DH1 3LE, United Kingdom

*Corresponding author Email: longxun.tang@outlook.com

Abstract: The Buchan Formation sandstone reservoirs from the Ardmore Field in the UK North Sea are fluvial-aeolian deposits and provide examples of porosity preservation in deeply-buried reservoirs (2.7 – 3.2 km) caused by grain-coating illite/smectite (I/S). Here, high reservoir quality commonly correlates with the occurrence of grain-coating I/S and consequent inhibition of quartz cementation in the aeolian dune and interdune sandstones. Porosity is lower in fluvial sandstones lacking grain coating I/S but with intense quartz overgrowths. We propose that the presence of I/S reflects concentration of the smectitic-rich clay bearing water which would have been the deposits of the interdune and/or distal sector of fluvial distributary system, and were introduced into aeolian deposits by mechanical infiltration. Petrographic relationships indicate that these coatings grew mainly before the mechanical compaction as the clays occur at grain contacts. The use of empirical model suggested that about 6 – 7% porosity have been preserved. The burial-thermal history of the Ardmore area contributed to the high quality reservoir because throughout much of the time since deposition, the Devonian sandstones have been little buried. Only from the Palaeogene the reservoir temperatures exceeded about 70°C and rapidly buried to today's maximum depth, which have minimized the negative effect generally ascribed to smectitic clays on reservoir quality. The circumstances of porosity preservation shown in this study may be unusual, but nonetheless have profound consequences for exploration. It is possible to identify new Buchan Formation prospects in areas hitherto dismissed because they were generally assumed to be poor reservoir.

Key words: Grain coating illite/smectite, Upper Devonian, Clay infiltration, Porosity preservation, UK North Sea

1. Introduction

Quartz cement is one of the dominant porosity reducing agents in many reservoir sandstones, but other factors such as grain size, sorting, clay content, mechanical compaction, pore fluid pressure, early cementation and authigenic clay minerals also play a critical role (Worden and Morad, 2000). Different types of grain coatings have been identified to inhibit or reduce quartz cementation. The basic mechanism of inhibiting quartz overgrowth is that the grain coatings covered the nucleation site on the host grains and the authigenic quartz could not nucleate on or through the coatings (Pittman, 1972). The most effective grain coating mineral is said to be micro-quartz (Aase et al., 1996) and for the grain coating clays, authigenic chlorite is commonly reported as a preserver (e.g. Pittman and Lumsden, 1968; Ehrenberg, 1993; Berger et al., 2009; Stricker and Jones, 2016). Illite is less frequently reported as grain coatings that preserve porosity (Storvoll et al., 2002) but frequently cited as the cause of permeability destruction (Robinson et al., 1993). Smectitic clay is commonly regarded as having negative effects on reservoir quality due to its water-sensitive swelling property (Gray and Rex, 1965), and it commonly transforms to fibrous/hairy illite in a potassium-rich pore fluids. Precipitation of illite usually causes significant permeability reduction (Almon and Davies, 1981; Le Gallo et al., 1998; Wilson et al., 2014).

The oil reservoirs in the Ardmore Field, UK Block 30/24, UK North Sea, are hosted in Permian Zechstein carbonates, Permian Rotliegend sandstones and Upper Devonian Buchan Formation sandstones (Gluyas et al., 2005). The two Permian units have been studied in a number of publications (e.g. Nagtegal, 1979; Glennie and Provan, 1990; Purvis, 1992; Howell and Mountney, 1997; Leveille et al., 1997; Sweet, 1999); however, the deeper and older Buchan Formation sandstones (2.7 – 3.2 km TVDSS) are poorly understood but have also been proven to be an important hydrocarbon reservoir in the North Sea (e.g. Edwards, 1991; Knight et al., 1993; Gambaro and Currie, 2003; Gluyas et al., 2005).

In this study, we discovered that the aeolian-associated sandstones with grain coating illite/smectite (I/S) usually have anomalously high porosity and permeability, while quartz overgrowth is almost absent in this sandstone type. Conversely, the fluvial facies without thick and continuous I/S coatings are usually cemented by extensive quartz overgrowth, and commonly show poor, or at best, moderate reservoir quality. Therefore, this study focused on the following points and questions: 1) why is the grain coating I/S only presented in aeolian sandstones and how did it form? and 2) is it possible to quantitatively evaluate the porosity preserving effect of I/S grain coatings? The positive effect of grain coating I/S can be expected to occur only under particular circumstances, but in such cases it can have profound consequences for exploration. This study has broad implications for future exploration, appraisal and production of Devonian reservoirs within this area.

2. Geological Setting

2.1 Tectonic Setting

The Ardmore Field is located on the Argyll Ridge, a large SW-NE trending Palaeozoic age tilted fault block on the south-western flank of the Central Graben in Block 30/24, UK North Sea, about 350 km south-east from Aberdeen. The field is located in a horst feature with the crest in the north and fault closure to the north-east. It measures 2.5 km wide and 6 km long (Fig. 1a). A combination of dip and faulting defines the limits of the field on the north-west and south-east flanks, while dip closure defines the southern limits of the field. The major fault trends are in two main directions, WNW–ESE cut by NE-SW faults (Fig. 1b). The top seal is provided by Triassic shale in the far west, Jurassic shale in the mid-part of the field and impermeable Chalk at the north-eastern crest (Gluyas et al., 2005). The trap relies heavily on the major NE-SW trending graben edge faults to the northeast and southwest of the field while dip closure occurs to the northwest and west.

2.2 Stratigraphy

The Devonian sequence in the Ardmore Field comprises a succession of the Middle Devonian Kyle limestone and Upper Devonian Buchan Formation. The succession dips to the south-west, and is separated from the Permian by a palaeo-topographic unconformity, in which successively younger stratigraphic units in the Devonian sub crop towards the south-west. Although the pre-Permian surface has topography it also dips to the SW, this has the effect of making the oldest part of the Buchan Formation subcrop the unconformity in the NE of the field and thus the youngest Devonian in the SW slightly deeper (Fig. 1b).

The Upper Devonian Buchan Formation comprises a thick, generally upward-coarsening succession of shales of mixed shallow marine and sabkha environment at the base, passing upwards into mainly fluvial and aeolian sandy sediments (Fig. 2). The whole Buchan succession lacks clear seismic stratigraphic markers, a combination of log and core data has been used to divide the stratigraphic units for the Upper Devonian group: B01 is the oldest unit overlying the Middle Devonian Limestone, and B11 is the youngest unit (Gluyas et al., 2005). In the absence of bio-stratigraphic data, sedimentary structures and lithofacies associations have been applied to help correlation (Gluyas et al., 2005). The total thickness of the Buchan Formation is not documented due to the combination of erosion below the Devonian-Permian unconformity, lateral thickness variation and incomplete well penetrations. The estimated thickness is about 250 – 800 m according to the seismic profile (Fig. 1c).

Units B01, B02, B03, B05 and B06 are equivocal about their origin due to the insufficient core coverage. The core description revealed the presence of two main sedimentary facies within the Buchan formation (Robson, 1991; Gluyas et al., 2005). Braided fluvial facies is the volumetrically major type (approx. 70%) and consists of multiple fining-upward sequences (not shown in the Fig. 2), each sequence is commonly composed of: 1) sand-supported

conglomerates at the cycle base with thickness around 0.5 – 1 m, the quartz and muddy clast pebbles (1 – 3 cm in diameter) are sub-angular to sub-rounded and show roughly imbricated alignment, which indicates the thin basal lag deposit within a channel (CHC); 2) fine to medium-grained, moderately sorted sandstones with trough cross bedding, planar cross bedding and horizontal laminations are the dominant type within the fining-upward cycle, representing various channel bar deposits (CHB) such as residual dunes, linguoid and transverse bars, and planar bed flows; and 3) laminated fine-grained sediments with soft sediment deformation usually form the top of the sequence, which indicate the decrease of flow velocity such as sand flat (SF) or channel abandonment (CHA) and usually occur at the top of the cycle with 0.5 m and up to 3 m thick.

The aeolian facies is the volumetrically minor type (approx. 30%) and composed of well sorted, medium-grained, pin-stripe laminated sandstones and fine-grained, discontinuous wavy laminated sandstones, which represents an interbedded dune (AD) and interdune (ID) deposits. Overall, the known units comprise a vertically fluvial (B04, approx. 100 m)-aeolian (B07 and B08, approx. 50 m)-fluvial (B09, B10 and B11, approx. 240 m) variation, which generally represents a progradation-retreat-progradation cycle of the alluvial fan-based braided system with aeolian deposits occurring mainly between two main progradation periods.

2.3 Previous study on Ardmore Field

The field is charged by Upper Jurassic Kimmeridge Clay in the northeast of Ardmore, which indicates these three reservoirs are in hydraulic connection (Gluyas et al., 2005). The Buchan Formation is composed chiefly of a sand-dominated unit deposited in a braided fluvial and aeolian environment during a hot and semi-arid to arid period (Gluyas et al., 2005; Kearsey et al., 2015). Gluyas et al. (2005) reported the conventional core analysis data for Buchan

Formation sandstones, porosity ranges between 1% and 28% while permeability varies between <1 mD and >5000 mD. The main influences on reservoir quality reduction were mechanical compaction, extensive quartz overgrowth and dolomite cementation (Bifani and Smith, 1985).

3. Dataset And Methodology

A total of 190 samples were taken from BGS and EnQuest core stores. Cores from five wells (30/24-05, 30/24-20z, 30/24-28, 30/24-31, 30/24-34) in the Buchan Formation ranging from 2650 m to 3150 m (TVDSS) were logged. The porosity and permeability data were provided by EnQuest internal reports. Porosity was determined via direct measurement of grain volume and bulk volume by helium expansion in a Boyle's Law porosimeter; the permeability data was determined by use of a nitrogen permeameter at a confining pressure of 400 psig and are Klinkenberg-corrected.

Thin-section petrography was used to determine the rock mineralogy, diagenetic features, pore types and clay distribution in the pore spaces. One hundred and one thin sections (14 from well 30/24-05, 16 from well 30/24-20z, 38 from well 30/24-28, 16 from well 30/24-31 and 17 from well 30/24-34) were used for petrographic analysis and point counting. The samples were impregnated with blue-dyed resin in order to identify porosity.

At least 300 points were counted in each thin section to identify detrital and authigenic phases, including the clay aggregates which are larger than 0.05 mm in size (pore space is excluded). This number of point counts per thin section has a standard deviation of 5.5% or less (at the 95% confidence level) for any measured volumetric percentage of mineral or porosity components (Stanton and Wilson, 1994). The point count results, petrographic information, and laboratory measured porosity/permeability are presented in Supplementary table 1.

Microstructural observation was obtained in both secondary and backscattered electron imaging, with a Hitachi SU70 scanning electron microscope (SEM). Typical voltage for thin sections was obtained at 15 Kev, 0.73 nA together with an analytical working distance of 15 mm. The electron microscope is equipped with an Oxford Instrument Aztec microanalysis system and Silicon drift (SDD) EDX detector X-max 50. Thin sections were carbon coated at 30 nm (Cressington Scientific 108 evaporating system A) in order to obtain large area "Phase Maps" which were achieved using Phase ID within Aztec 3.3 software. Rock chip samples from both fluvial and aeolian sandstones were Au/Pd coated at 35 nm (Cressington Scientific 108 Auto sputter coater) for optimum imaging resolution at 5 to 8 Kev.

To identify and quantify the clay mineralogy, six samples were chosen for XRD analysis (4 from grain coated aeolian sandstone samples, 2 from fluvial sandstone samples with quartz and dolomite cements and without grain coatings). The bulk rock was disaggregated by gentle crushing and suspend in distilled water. After allowing the coarse grains to settle for 3 hours, the clay in suspension was decanted in the centrifuge for 4.8 minutes at 1000 rpm, and this process is performed 3 times. Clay with less than 2 microns was tested after being air dried, solvation with glycerol and heating at 500°C for 2 hours.

4. Results

4.1 General Petrographic Descriptions

4.1.1 Detrital mineralogy

The studied Buchan Formation sandstones are litharenite to sub-litharenite and minor quartz-arenite based on Folk (1957), with an overall average composition of $Q_{78.3}F_{2.9}R_{18.8}$. The average composition for fluvial sandstones is $Q_{76.1}F_{3.3}R_{20.7}$ (Fig. 3a); aeolian sandstones have an average composition of $Q_{82.1}F_{2.4}R_{15.6}$ (Fig. 3b). Texturally, the fluvial sandstones are

relatively immature and fine to medium grained, sorting ranges from poor to moderate and roundness of grains varies from sub-angular to sub-rounded. Grains are tightly compacted showing long and curved grain contacts. Conversely, the fine to medium grained aeolian sandstones are more mature, sorting ranges from moderate to good and roundness of grains varies from sub-rounded to rounded, and the grain contacts are commonly point to long.

In all samples, quartz is the dominant grain type (25 – 92.5%). Most quartz grains are monocrystalline (Fig. 4a), some of them showing little to moderate undulose extinction (Fig. 4b). Polycrystalline quartz is a minor constituent and only found in fine pebble grains (Fig. 4c). Feldspar is commonly present in trace amount and up to 7%, the main type is microcline with polysynthetic twinning (Fig. 4d). The feldspars occur as both fresh (Fig. 4d) and kaolinitized grains (Fig. 4e). Most mica grains are muscovite presenting in all the samples and comprising up to 13%. Micas show variable amounts of distortion (Fig. 4b). Rock fragments (Fig. 4f) are mainly micaceous and illitic mud clasts, fine-grained metamorphic and volcanic fragments are present in trace quantities. The abundance of rock fragments is highly variable (1 – 69%) and related to different sub-facies: CHB have lower average rock fragments (11%) among all fluvial sub-facies (15% in CHC, 16% in SF and 27% in CHA). In the aeolian facies, aeolian dune sandstones have a lower average rock fragments (13%) than the interdune deposits (16%).

In both fluvial and aeolian sandstones, pore space mainly consists of primary intergranular pores, secondary inter- and intragranular pores and intra-crystalline micro pores. The polygonal intergranular pores are the main type (more than 90% among all pore space) and range in sizes from 5 – 200 μm. The secondary pores (less than 10% among all pore space) are mainly contributed from framework-grain dissolution (e.g. dissolution of detrital feldspars), and dissolution of dolomite cement can be found in trace amounts. The intra-

crystalline micro pores (negligible among all pore space) mainly consist of micro pores in clay minerals (e.g. kaolinite, illite, smectite) and range in size from 0.1 – 5 μm.

4.1.2 Authigenic mineralogy

Authigenic minerals in the studied sandstones are mainly dolomite, quartz overgrowth, kaolinite, illite and I/S. The kaolinite, illite and quartz overgrowth are usually associated with fluvial sandstones, while I/S are only found in aeolian sandstones.

Dolomite is the prevalent cement in the Buchan Formation sandstones ranging from 0 – 36% with an average value of 5.7%, and are commonly iron-stained. It is usually presented as thin bands of disseminated red-brown stained nodules in hand specimen with a size of up to 2 mm (Fig. 5a). Thin section observation reveals a rhombic shape with clear rims and cloudy centre (Fig. 5b) and poikilotopic structure (Fig. 5c).

Quartz overgrowth is present primarily as syntaxial cement forming incomplete or complete rims around quartz grains (Figs. 4a and 5d). Boundaries between detrital quartz grains and overgrowth cements are visible due to the presence of inclusions along grain boundaries. Quartz overgrowths are widely distributed in the fluvial sandstone samples (up to 6%, average 3%) and is almost absent in aeolian samples, except a few of them (5 out of 36) have trace amount of quartz overgrowth up to 1% (Supplementary table 1). Kaolinite and authigenic illite are the two main clay types in fluvial sandstones. Kaolinite ranges from 0% and up to 15% with an average amount of 6%, mainly occurs as euhedral pseudo-hexagonal plates and vermicular or booklet aggregates filling primary pores (Fig. 5e). In the aeolian sandstones, kaolinite is in minor amount ranged from 0% to 6% (average 2%). Illite has a range from 0% and up to 7% with an average amounts of 2% and occurs as fibrous or hairy crystals mainly nucleated on kaolinite (Fig. 5f) and shows a pore-bridging habit (Fig. 5g).

Illite/smectite (I/S) has been identified by XRD (Table. 1) and EDX analysis (Fig. 5k). It is the most important clay type in the studied aeolian sandstones although it is only present in minor amounts (0.5 – 5%). The thin section and SEM observations illustrate that the I/S is presenting in two forms: 1) grain coating I/S (Figs. 5h, 5i) commonly occurs as cornflake or honeycomb morphology with filamentous terminations, and consists of a 1 – 5 μm thick rim coating all the detrital grains in aeolian sandstones; it is absent in fluvial sandstones. It is also observed that quartz overgrowth are absent in aeolian sandstones where uniform and robust grain coating I/S has developed; and 2) pore-filling I/S (Fig. 5i, 5j), commonly presenting as flocculent aggregates existing in the intergranular pore space of aeolian sandstones, and is also absent in fluvial sandstones. To evaluate the development, coverage and continuity of the grain coating I/S, the mineral phase map has been created for a typical aeolian dune sample (Figs. 6a and 6b). Figure 6b clearly displayed that nearly all the grains are coated by well-developed and continuous grain coating I/S, the visual grain coating coverage is nearly 100%.

In both sandstone types, chlorite is subordinate and present in trace amounts (0.1 - 0.5%) which is confirmed by XRD analysis (Table 1).

4.2 Porosity and Permeability

The Buchan Formation sandstones have a wide range of porosity and permeability (ϕ = 1 – 28% and K= 0.1 – 5290 mD). Porosity and permeability are well correlated in most of the samples (in fluvial samples, R^2= 0.68; in aeolian samples, R^2= 0.89; in all samples, R^2= 0.74) inferred that the factors affecting porosity would also affect permeability (Fig. 7a).

For the fluvial units including B04, B09, B10 and B11 (Figs. 7b-7e), the porosity ranges from 0.1% to 23.1% (arithmetic mean 12.7%), and the permeability ranges from 0.2 mD to 1240 mD (arithmetic mean 147.7 mD, geometric mean 5.41 mD). For the aeolian units B07

and B08 (Fig. 7f), the porosity ranges from 5.1% to 28% (arithmetic mean 20.2%), and the permeability ranges from 0.2 mD to 5290 mD (arithmetic mean 740.6 mD, geometric mean 64.9 mD).

4.3 Porosity loss evaluation

Calculation on porosity loss from compaction (COPL) and cementation (CEPL) is a good way to calculate the effect of compaction and cementation on reducing porosity. These two parameters were firstly proposed by Lundergard (1992), and a useful parameter compaction index (Ic), can be calculated using following equations:

$$\mathrm{COPL} = \mathrm{P_i} - \left(\frac{(100-\mathrm{P_i})\times \mathrm{IGV}}{100-\mathrm{IGV}}\right). \quad (1)$$

$$\mathrm{CEPL} = (\mathrm{P_i} - \mathrm{COPL}) \times \left(\frac{\mathrm{C}}{\mathrm{IGV}}\right). \quad (2)$$

$$\mathrm{Ic} = \frac{\mathrm{COPL}}{\mathrm{COPL+CEPL}}. \quad (3)$$

Where P_i is the assumed initial porosity, the intergranular volume (*IGV*) is calculated by adding up the measured porosity and the total cement volume *C*. The calculation of COPL and CEPL are only accurate when three conditions are met: 1) the assumed initial porosity *Pi* is appropriate; 2) the amount of cement produced by local grain dissolution is negligible or known; and 3) the amount of framework exported by dissolution is negligible or known (Lundergard, 1992). The compaction index (Ic) equals 1.0 when all porosity loss is due to mechanical compaction, and equals 0.0 when all porosity loss is due to cementation. In this study, we employ the estimated *Pi* for loose sand according to Beard and Weyl (1973), the assumed *Pi* for the fine-medium grained, moderately sorted fluvial sandstones is 34.8%, and for the fine-medium grained, well sorted aeolian sandstones, Pi is 37.8%.

The results (Supplementary table 2) show that compaction has reduced more porosity in aeolian sandstones than in fluvial sandstones: the COPL value is 14.82% (accounted for

39.21% on initial porosity, average Ic = 0.73) in aeolian sandstone samples. 10.06% (accounted for 28.91% on initial porosity, average Ic = 0.44) in fluvial sandstone samples, respectively. It is also worthy to note that the COPL of fluvial samples has a larger range (0 – 29%) than aeolian samples (3.5 – 22.8%).

The CEPL results suggest that fluvial sandstones suffered much more porosity loss from cementation (average 12.71%, accounted for 36.52% on initial porosity) than aeolian sandstones (average 5.63%, accounted for 14.89% on initial porosity).

4.4 Burial-thermal history

The 1D burial history was modelled using Schlumberger petroleum systems modelling software PetroMod (V2014.1). Several heat flow histories of the Central Graben, to be more specifically, UK Quadrant 30 in the UK North Sea have been employed for the modelling (Swarbrick et al., 2000; Carr, 2003; Di Primio and Neumann, 2008). Figure 8 is a burial-temperature history for the Buchan Formation in the Ardmore Field which is generally similar to burial histories presented in other studies of Central Graben (Nguyen et al., 2013). The Buchan Formation in the Ardmore Field was at consistently shallow burial depth and low temperature (< 1.5 km and < 70°C) until Paleogene, and then rapidly buried into current maximum depth (2.7 – 3.2 km) and temperature (approx. 115°C) within a short period (less than 70 million years).

5. Paragenesis

The relative timing of the main diagenetic features can be reconstructed by considering the relationships between the different diagenetic events (Fig. 9). However, there are some diagenetic differences between fluvial and aeolian sandstones.

The earliest diagenetic event was the formation of grain coating clays in aeolian deposits, which is considered to be introduced from the infiltration of clay-bearing groundwater through the sands. This event was prior to the compaction and could be proved by the presence of grain coating clays at grain contacts (Figs. 6b and 10).

Mechanical compaction in both aeolian and fluvial deposits followed after clay infiltration, during which mica flakes were deformed around quartz and feldspar grains (Fig. 4b). In both fluvial and aeolian samples, an early dolomite cementation occurred at this time, as in some samples the detrital grains appear to float and point grain contact is preserved within the poikilotopic dolomite cement (Fig. 5c). Where dolomite is not present, grains are well compacted (Fig. 5c). The presence of euhedral dolomite with cloudy centres and clear rims (Fig. 5b) might be an indicator of dolomitization occurred on calcrete precursor. Pressure dissolution at quartz grain contacts would have occurred as compaction increased due to the weight of overburden. This is more common in fluvial sandstones possibly due to the greater abundance of rock fragments, such as ductile micaceous clasts, may promote the compaction in the fluvial sandstones and resulted in concavo-convex grain contacts (Fig. 5c). This is also supported by greater maximum COPL value in fluvial samples (29%) than in aeolian samples (22.8%).

A subsequent event was the dissolution of feldspar in both aeolian and fluvial deposits which generated authigenic kaolinite (Fig. 4e). Considerable silica ions were released into solution which would form quartz overgrowth in fluvial sandstones, and the pressure dissolution is another possible silica source but only has minor contributions (Tang et al., 2018). This process is usually suggested to be occur in middle to late diagenetic stage (Worden and Morad, 2000). While in the aeolian sandstones, the presence of early-formed grain coating clays provided no site on the grain surface for nucleation of silica ions, quartz overgrowth is thereby almost absent.

313 The whole diagenetic setting might become more alkaline during late diagenesis. In the
314 fluvial sandstone, illitization occurred on kaolinite displaying a fibrous/hairy morphology
315 (Fig. 5f). In the aeolian sandstones, illitization is observed both on grain-coating and pore-
316 filling smectite (Fig. 5i). The presence of pore-bridging habit of illite is often regarded to be
317 an indicator of intermediate to deeper burial (Jiang, 2012). It can also be supported by XRD
318 data (Table 1), the I/S is in R1 ordered interstratification and the percentage of illite within
319 I/S is around 70 – 80%, this usually indicates a temperature condition of 100 – 110°C (e.g
320 Hoffman and Hower, 1979; Huang et al., 1993). There are also minor chloritization due to the
321 presence of Mg^{2+} probably originated from the subsequent dolomite dissolution.

322 **6. Discussion**

323 **6.1 Source of grain coating I/S**

324 The cornflake or honeycomb morphology observed under SEM suggests that the grain
325 coating I/S (also the pore-filling I/S) was transformed from smectitic precursor, as illite
326 originated from kaolinite is more possible to show sheet-like morphology (Pollastro, 1985).
327 Mineralogically, Pittman (1992) deduced that smectite could form an effective dense and
328 continuous grain coat because they nucleate flatly attached to the detrital grain surface and
329 curl away from that surface, the clay developed initially as clay wisps and progressed to clay
330 platelets that formed a root zone, then to an open polygonal box-work and finally to a denser
331 polygonal box-work.
332 In this study, the grain coating I/S has a contrasting distribution pattern that it is only
333 found in aeolian sandstones and absent in fluvial sandstones. Within the given arid/semi-arid
334 aeolian-dominated setting, the fine-grained sandstones with discontinuous wavy laminations
335 commonly indicate a wet interdune or desert lake deposits, which were possibly charged by
336 distal of fluvial distributary system sector (i.e. sand flat) during fluvial-retreat period. As a

consequence, the fine-grained sediments, in this case smectitic clays, would be accumulated in this setting and flow into aeolian dune by mechanical infiltration, which is suggested to be a likely main source of grain coating and pore-filling I/S.

Petrographic evidence also supports this idea. Wilson (1992) has set several criteria for recognizing mechanically infiltrated clay rims in aeolian and shallow marine sandstones: 1) presence at grain contacts; 2) increased thickness in depressions on framework-grain surface; and 3) more extensive development in finer grained laminae or beds. In this study, the petrographic features of grain coating I/S meet the recognition criteria of mechanical infiltration, it occurs at the grain contacts of aeolian sandstones, and generally shows a thicker I/S coating in the framework-grain depressions and rough surfaces than the non-depression and smooth areas (Fig. 10). Additional evidence from pinstripe laminated dune sandstones clearly displays that more extensive development of grain coating and pore-filling I/S occurred in finer-grained aeolian sands than in medium-grain aeolian sands (Fig. 11).

6.2 Effect of grain coating I/S on reservoir quality

The sum of total cements (dolomite, quartz overgrowth and authigenic clays) clearly has an inverse relationship ($R^2 = 0.47$) with porosity (Fig. 12); this at least indicates that the various types of cementation are jointly the main control of reservoir quality. As the dolomite and authigenic kaolinite occurred in both fluvial and aeolian sandstones, the most remarkable difference between two sandstone types is the quartz overgrowth which is extensively distributed (up to 6%) in fluvial sandstones and nearly negligible in aeolian sandstones.

Continuous grain coating minerals are often the key factor for high porosity in deeply buried (> 2.5 km) sandstones (Pittman et al., 1992). Amongst the numerous studies, the grain coating chlorite and microcrystalline quartz are most frequently mentioned (e.g. Pittman and Lumsden, 1968; Ehrenberg, 1993; Aase et al., 1996; Stricker and Jones, 2016). In our study, the grain coating I/S is also effective on inhibiting quartz overgrowth thus preserving porosity.

In the Buchan Formation, the amount of quartz cement in all the samples is clearly linked to the presence and coverage of grain coating I/S. The fluvial sandstones do not contain any type of continuous and well developed clay coatings around quartz grains (in the selected sample, grain coverage is nearly 0%, n = 89) and are hence 95% of grains (84 out of 89) are cemented by quartz overgrowth in variable amount (Fig. 13a). Conversely, grain coating I/S are well developed in almost all the aeolian sandstone samples with good coverage (in the selected sample, grain coverage = 100%, n = 212) and continuity, and the quartz cementation is almost absent (Fig. 13b). To quantitatively evaluate the effect of grain coating I/S, we employ the algorithm of Ehrenberg (1993) to calculate the theoretical amount of quartz cementation in upper fine to medium-grained (grain size set as 0.25 mm – 0.3 mm) aeolian sandstones if the grain coating I/S were absent. With the assumed duration of 70 million years from beginning of Palaeogene, the result shows there would be about 6 – 7% porosity has been preserved by grain coating I/S (Fig. 14).

The grain coating I/S in this study was transformed from smectitic precursor. For the reservoir quality, smectitic clay usually has two shortcomings: 1) smectite would transform to mixed layer smectite-illite and finally illite when the K^+ is enriched in the fluid and temperature reaches around 70 – 80°C or higher. The hairy/fibrous morphology of illite would reduce the pore and throat space, thus significantly decreasing reservoir quality, especially permeability (e.g. Almon and Davies, 1981; Wilson and Stanton, 1994; Le Gallo et al., 1998); 2) smectite has a high water sensitivity thus could easily swell and occupy the pore space (Gray and Rex, 1965).

However, these two shortcomings have very limited impact on reservoir quality in this study. Huang et al. (1993) and Wilson and Stanton (1994) suggested that the kinetics of illitization on precursor detrital smectitic clays not solely depends on temperature but potassium concentration and total time-temperature exposure. In the Buchan Formation,

feldspar dissolution might provide considerable amount of K^+. The burial history has illustrated that the Buchan Formation were consistently at shallow depth (< 1.5 km, temperature < 70°C) until the Palaeogene and was then rapidly buried to present day maximum burial depth. This rapid burial would only provide short thermal exposure which is insufficient for full and complete illitization. Secondly, the amount of pore-filling I/S are commonly less than 5% in aeolian sandstone samples and this would not significantly occlude the pore space.

Conclusions

The grain coatings observed in the fluvial-aeolian Buchan Formation sandstones of the Ardmore Field have been identified as illite/smectite (I/S) which were transformed from smectite precursor. The effect of porosity preservation due to grain coating chlorite and microcrystalline quartz has been demonstrated in a number of publications, this study shows that I/S coatings can also be very effective in preventing quartz cementation under specific conditions, and thereby help preserving primary porosity.

In the fluvial sandstones, the precursor material has been absent resulting in the absence of clay coatings on the sand grains, and thereby quartz cementation is extensively developed and reservoir quality is poorer.

The thick and continuous grain coating I/S with extensive grain coverage is only observed in aeolian sandstones and this clay coating has inhibited quartz overgrowth and hence high porosity values have been persevered at more than 2.5 km burial depth. The illitization on smectite occurred limitedly thus would not significantly reduce reservoir quality. This is mainly due to the featured burial history: the Buchan Formation was at consistently shallow depth and low temperature until Palaeogene which is not kinetically favourable to activate the smectite illitization. After the Palaeogene, the Buchan Formation was buried to today's

maximum depth and temperature rapidly, the short time-temperature exposure is insufficient for full and complete illitization. The I/S coatings were generated from smectitic precursor. It is possible that the precursor has been formed by mechanical infiltration from associated damp interdune deposits possibly charged by clay-bearing water representing distal sector of fluvial distributary system during aeolian-dominated period.

The understanding of the positive effect on porosity preservation from grain-coating I/S may aid predictions of high quality Devonian-hosted reservoirs in the North Sea. Such sandstones could form attractive exploration targets that hitherto may have been ignored because they would be expected to have low porosity on the basis of regional trends.

Acknowledgments

The author thanks CGG for providing the seismic data; Enquest PLC for supporting this research through access to core and financial support of analytical work; X-ray Mineral Services Ltd for processing the XRD analysis; Dr Bernard Besly for providing data and helpful discussions; BGS (British Geological Survey) for its assistance in facilitating the examination of Devonian cores. We are all grateful for the expertise and general assistance offered by Mr Ian Chaplin (Department of Earth Sciences, Durham University) and Mr Leon Bowen (Department of Physics, Durham University) in the preparation of samples.

REFERENCES

Aase, N.E., Bjorkum, P.A. and Nadeau, P.H., 1996. The effect of grain-coating microquartz on preservation of reservoir porosity. AAPG Bulletin, 80(10): pp. 1654-1673.

Almon, W.R. and Davies, D.K., 1981. Formation damage and the crystal chemistry of clays. Short course in clays and the resource geologist: Montreal, Mineralogical Association of Canada, 7: pp. 81-102.

Beard, D. and Weyl, P., 1973. Influence of texture on porosity and permeability of unconsolidated sand. AAPG Bulletin, 57(2): pp. 349-369.

437 Berger, A., Gier, S. and Krois, P., 2009. Porosity-preserving chlorite cements in shallow-marine
438 volcaniclastic sandstones: Evidence from Cretaceous sandstones of the Sawan gas field,
439 Pakistan. AAPG Bulletin, 93(5): pp. 595-615.
440 Bifani, R. and Smith, C., 1985. The Argyll field after a decade of production. Society of Petroleum
441 Engineers Journal, SPE-13987-MS: pp. 1-32.
442 Carr, A., 2003. Thermal history model for the South Central Graben, North Sea, derived using both
443 tectonics and maturation. International Journal of Coal Geology, 54(1): pp. 3-19.
444 Di Primio, R. and Neumann, V., 2008. HPHT reservoir evolution: a case study from Jade and Judy
445 fields, Central Graben, UK North Sea. International Journal of Earth Sciences, 97(5): pp.
446 1101-1114.
447 Edwards, C., 1991. The Buchan Field, Blocks 20/5a and 21/1a, UK North Sea. In: I.L. Abbotts
448 (Editor), United Kingdom Oil and Gas Fields, 25 Years Commemorative Volume. 14.
449 Geological Society, London, pp. 253-259.
450 Ehrenberg, S., 1993. Preservation of anomalously high porosity in deeply buried sandstones by grain-
451 coating chlorite: examples from the Norwegian continental shelf. AAPG Bulletin, 77(7): pp.
452 1260-1286.
453 Folk, R.L., 1957. Petrology of sedimentary rocks. Hemphill Publishing Company, pp. 63.
454 Gambaro, M. and Currie, M., 2003. The Balmoral, Glamis and Stirling fields, block 16/21, UK
455 Central North Sea. In: J.G. Gluyas and H.M. Hichens (Editors), United Kingdom Oil and Gas
456 Fields Commemorative Millennium Volume. 20. Geological Society, London, pp. 395-413.
457 Glennie, K. and Provan, D., 1990. Lower Permian Rotliegend reservoir of the southern North Sea gas
458 province. In: J. Brooks (Editor), Geological Society Special Publications: Classic Petroleum
459 Provinces. 50. Geological Society, London, pp. 399-416.
460 Gluyas, J.G., Mair, B., Schofield, P., Arkley, P. and McRae, D., 2005. Ardmore Field: rebirth of the
461 first offshore oil field, UKCS, Geological Society, London, Petroleum Geology Conference
462 series. Geological Society of London, pp. 367-388.
463 Gray, D. and Rex, R., 1965. Formation damage in sandstones caused by clay dispersion and migration.
464 In: A. Swineford (Editor), Clays and Clay Minerals: Proceedings of the Fourteenth National
465 Conference. pp. 355-365.
466 Hoffman, J. and Hower, J., 1979. Clay mineral assemblages as low grade metamorphic
467 geothermometers: application to the thrust faulted disturbed belt of Montana, USA. In: P.A.
468 Scholle, & Schluger, P. R. (Editor), Special Publications of SEPM: Aspects of diagenesis:
469 based on symposia. 26, pp. 55-79.
470 Howell, J. and Mountney, N., 1997. Climatic cyclicity and accommodation space in arid to semi-arid
471 depositional systems: an example from the Rotliegend Group of the UK southern North Sea.
472 In: K. Ziegler, P. Turner and S.R. Daines (Editors), Geological Society Special Publications:
473 Petroleum Geology of the Southern North Sea: Future Potential. 123. Geological Society,
474 London, pp. 63-86.
475 Huang, W.-L., Longo, J.M. and Pevear, D.R., 1993. An experimentally derived kinetic model for
476 smectite-to-illite conversion and its use as a geothermometer. Clays and Clay Minerals, 41: pp.
477 162-162.
478 Jiang, S., 2012. Clay minerals from the perspective of oil and gas exploration. In: M. Valaškova and
479 G.S. Martynkova (Editors), Clay Minerals in Nature-Their Characterization, Modification and
480 Application. InTech, pp. 21-38.
481 Kearsey, T., Ellen, R., Millward, D. and Monaghan, A., 2015. Devonian and Carboniferous
482 stratigraphical correlation and interpretation in the Central North Sea, Quadrants 25–44.
483 British Geological Survey (CR/15/117N) (Unpublished): pp. 1-80.
484 Knight, I., Allen, L., Coipel, J., Jacobs, L. and Scanlan, M., 1993. The Embla Field, Geological
485 Society, London, Petroleum Geology Conference series. Geological Society of London, pp.
486 1433-1444.
487 Le Gallo, Y., Bildstein, O. and Brosse, E., 1998. Coupled reaction-flow modeling of diagenetic
488 changes in reservoir permeability, porosity and mineral compositions. Journal of Hydrology,
489 209(1): pp. 366-388.
490 Leveille, G.P., Primmer, T.J., Dudley, G., Ellis, D. and Allinson, G.J., 1997. Diagenetic controls on
491 reservoir quality in Permian Rotliegendes sandstones, Jupiter Fields area, southern North Sea.

In: K. Ziegler, P. Turner and S.R. Daines (Editors), Geological Society Special Publications: Petroleum Geology of the Southern North Sea: Future Potential. 123. Geological Society, London, pp. 105-122.
Lundergard, P., 1992. Sandstone porosity loss. A ‘‘big picture’’view of the importance of Compactation. Journal of Sedimentary Petrology, 62: pp. 250-260.
Nagtegal, P., 1979. Relationship of facies and reservoir quality in Rotliegendes desert sandstones, southern North Sea region. Journal of Petroleum Geology, 2(2): pp. 145-158.
Nguyen, B.T., Jones, S.J., Goulty, N.R., Middleton, A.J., Grant, N., Ferguson, A. and Bowen, L., 2013. The role of fluid pressure and diagenetic cements for porosity preservation in Triassic fluvial reservoirs of the Central Graben, North Sea. AAPG Bulletin, 97(8): pp. 1273-1302.
Pittman, E.D., 1972. Diagenesis of quartz in sandstones as revealed by scanning electron microscopy. Journal of Sedimentary Petrology, 42(3): pp. 507-519.
Pittman, E.D., Larese, R.E. and Heald, M.T., 1992. Clay coats: Occurrence and relevance to preservation of porosity in sandstones. In: D.W. Houseknecht and E.D. Pittman (Editors), Special Publications of SEPM: Origin, Diagenesis, and Petrophysics of Clay Minerals in Sandstones. 47, pp. 241-255.
Pittman, E.D. and Lumsden, D.N., 1968. Relationship Between Chlorite Coatings on Quartz Grains and Porosity, Spiro Sand, Oklahoma: NOTES. Journal of Sedimentary Petrology, 38(2): pp. 668-670.
Purvis, K., 1992. Lower Permian Rotliegend sandstones, southern North Sea: a case study of sandstone diagenesis in evaporite-associated sequences. Sedimentary Geology, 77(3-4): pp. 155-171.
Robinson, A., Coleman, M.L. and Gluyas, J.G., 1993. The age of illite cement growth, Village Fields area, southern North Sea: Evidence from K-Ar ages and 18O/16O ratios. AAPG Bulletin, 77(1): pp. 68-80.
Robson, D., 1991. The Argyll, Duncan and Innes Fields, Block 30/24 and 30/25a, UK North Sea. In: I.L. Abbotts (Editor), United Kingdom Oil and Gas Fields, 25 Years Commemorative Volume. 14. Geological Society, London, pp. 219-226.
Stanton, P.T. and Wilson, M.D., 1994. Measurement of Independent Variables-Composition. In: M.D. Wilson (Editor), Special Publications of SEPM: Reservoir Quality Assessment and Prediction in Clastic Rocks (SC30). Short Course Notes, pp. 277-290.
Storvoll, V., Bjørlykke, K., Karlsen, D. and Saigal, G., 2002. Porosity preservation in reservoir sandstones due to grain-coating illite: a study of the Jurassic Garn Formation from the Kristin and Lavrans fields, offshore Mid-Norway. Marine and Petroleum Geology, 19(6): pp. 767-781.
Stricker, S. and Jones, S.J., 2016. Enhanced porosity preservation by pore fluid overpressure and chlorite grain coatings in the Triassic Skagerrak, Central Graben, North Sea, UK. In: P.J. Armitage, A.R. Butcher, J.M. Churchill, A.E. Csoma, C. Hollis, R.H. Lander, J.E. Omma and R.H. Worden (Editors), Geological Society Special Publications: Reservoir Quality of Clastic and Carbonate Rocks: Analysis, Modelling and Prediction. 435, pp. 1-21.
Swarbrick, R., Osborne, M., Grunberger, D., Yardley, G., Macleod, G., Aplin, A., Larter, S., Knight, I. and Auld, H., 2000. Integrated study of the Judy Field (Block 30/7a)—an overpressured Central North Sea oil/gas field. Marine and Petroleum Geology, 17(9): pp. 993-1010.
Sweet, M., 1999. Interaction between aeolian, fluvial and playa environments in the Permian Upper Rotliegend Group, UK southern North Sea. Sedimentology, 46(1): pp. 171-188.
Tang, L., Gluyas, J.G. and Jones, S.J., 2018. Diagenetic and geochemical studies of the Buchan Sandstone (Upper Devonian) in the Central North Sea. Petroleum Science, in press.
Wilson, M.D., 1992. Inherited grain-rimming clays in sandstones from eolian and shelf environments: their origin and control on reservoir properties. In: D.W. Houseknecht and E.D. Pittman (Editors), Special Publications of SEPM: Origin, Diagenesis, and Petrophysics of Clay Minerals in Sandstones. 47, pp. 209-225.
Wilson, M.D. and Stanton, P.T., 1994. Diagenetic mechanisms of porosity and permeability reduction and enhancement. In: M.D. Wilson (Editor), Special Publications of SEPM: Reservoir Quality Assessment and Prediction in Clastic Rocks (SC30). Short Course Notes, pp. 59-118.

Wilson, M.J., Wilson, L. and Patey, I., 2014. The influence of individual clay minerals on formation damage of reservoir sandstones: a critical review with some new insights. Clay Minerals, 49(2): pp. 147-164.
Worden, R.H. and Morad, S., 2000. Quartz Cementation in Oil Field Sandstones: A Review of the Key Controversies. In: R.H. Worden and S. Morad (Editors), International Association of Sedimentologists Special publication: Quartz cementation in sandstones. 29, pp. 1-20.

APPENDIX

Supplementary table 1. Petrography information of the Buchan Formation samples in Ardmore field, note the well names and locations are shown in Fig. 1a in bold.

Supplementary table 2. Total cement volume (C), measured porosity (Pm), intergranular volume (IGV), porosity-loss by mechanical compaction (COPL) and porosity-loss by cementation (CEPL) all in% for the aeolian dune and braided channel samples

LIST OF TABLES AND FIGURES

Q-quartz; Qu- quartz grains with undulose extinction; PQ- Polycrystalline quartz; F-feldspar; C-carbonate cement; K-kaolinite; RF-rock fragment

Fig. 5. Photomicrographs showing different diagenetic minerals. (a) Thin bands of 'spotty' red-brown stained cements (yellow arrows) in the cores. Well 30/24-05, 2849.1 m, unit B04, fluvial facies; (b) Dolomite cements in the pore space showing well rhombic shape with cloudy core and light rims, cross-polarized light, well 30/24-05, 2849.1 m, unit B04, fluvial facies; (c) Quartz grains floating in the dolomite cements and well compacted (white arrows) without pore-filling dolomite cements, cross-polarized light, well 30/24-20z, 3126 m, unit B04, fluvial facies; (d) Extensive quartz overgrowth (red arrows) on the detrital quartz grains, cross-polarized light, well 30/24-20z, 3126 m, unit B04, fluvial facies; (e) Kaolinites showing pseudo-hexagonal plates and vermicular and booklet morphologies under SEM. Well 30/24-20z, 3176.6 m, unit B04, fluvial facies; (f) Fibrous/hairy authigenic illite based on kaolinite under SEM. Well 30/24-20z, 3126 m, unit B04, fluvial facies; (g) SEM image showing pore-bridging habit of authigenic illite (yellow arrows). Well 30/24-20z, 3165.3 m, fluvial facies; (h) Grain coating clays existing at grain contacts (white arrows), plane- polarized light ,well 30/24-31, 3197.7 m, unit B08, aeolian facies; (i) Pore-filling and grain coating smectite-illite mixed layers showing honeycomb or cornflake morphology under SEM. Well 30/24-28, 2891.6 m, unit B07, aeolian facies; (j) Enlarged view of the rectangle area in Fig. 6i, note the filamentous terminations (white arrows) indicates the illitization occurred; (k) EDX spectrum of the rectangle area in Fig. 6j, note the small peak of potassium indicates the partial illitization.

D-dolomite; P-pore space; K-kaolinite; I-illite; I/S-illite/smectite

Fig. 6. The mineral phase map of a typical aeolian dune sandstone sample which contain well-developed and continuous grain coating clays. (a) BSEM image of the thin section; (b)

Grain coating phase map. Sample from Well 30/24-28, 2891.6 m, unit B07, aeolian dune facies.

Fig. 7. Porosity and permeability distributions and correlation coefficients for: (a) All the samples; (b) Stratigraphic unit B04; (c) Stratigraphic unit B09; (d) Stratigraphic unit B10; (e) Stratigraphic unit B11; (f) Stratigraphic units B07 and B08.

Fig. 8. 1D burial depth curve with geothermal isochore lines of Buchan Formation in the Ardmore Field.

Fig.9. Paragenetic sequences of the Buchan Formation, the solid/dash lines represent the major/minor events. Note the superscripts at the end of each event represent: A – the event mainly occurred in aeolian sandstones; F – the event mainly occurred in fluvial sandstones; A&F – the event mainly occurred in both aeolian and fluvial sandstones; * – the event is not observed under either thin section or SEM, but confirmed by XRD.

Fig. 10. The photomicrograph (plane-polarized light) illustrates the presence of grain coating I/S in the grain contact areas (white arrows), thicker coats in grain surface depressions (yellow arrows) and grain rough surface (red arrows), and thinner coats in non-depression areas (black arrows). Sample from well 30/24-31, 3190.6 m, unit B08, aeolian dune sands.

Fig. 11. Photomicrograph illustrating different abundance of infiltrated clays in a representative pin-stripe lamination dune sandstone sample. Note the finer grain-size lamentation (right) clearly contains more pore-filling clays. Well 30/24-31, 3190.6 m, unit B08, aeolian dune sands.

Fig. 12. The scattered porosity and total cements showing a clearly inverse relationship. The data is categorized by aeolian and fluvial facies.

Fig. 13. Comparison between: (a) Fluvial channel sandstone without clay coatings which is extensively cemented by quartz overgrowth, the clay coating coverage is 0%, and about 95% of grains have quartz overgrowth, n = 89. Well 30/24-20z, 3117.8 m, unit B04; (b) Aeolian sandstone with very high clay coating coverage (100%, n = 212) with no quartz overgrowth. Well 30/24-31, 3202.2 m, unit B08. Both figures were taken under plane-polarized light.

Fig. 14. Empirical calculation of possible quartz overgrowth amounts for sand grain size in 0.25 and 0.30 mm during 70 million years. The algorithm is after Ehrenberg (1993).

651 **Table**

652 **Table 1.** XRD data for <2μm size mineral fraction in selected samples

Well	Depth (m)	Facies	Wt.%	Illite/smectite				Illite			Kaolinite			Chlorite			Quartz		Calcite		Dolomite	
			<2um	% A	% B	Order	% I	% A	% B	Crys	% A	% B	Crys	% A	% B	Crys	% A	% B	% A	% B	% A	% B
30/24-28	2790.1	AD	1.9	34.4	0.7	O	70-80	58.3	1.1	P	0.0	0.0	-	7.1	0.1	P	0.3	0.1	0.0	0.0	0.0	0.0
30/24-28	2829.8	AD	3.0	46.3	1.4	O	70-80	25.9	0.8	P	22.6	0.7	M	2.9	0.1	M	2.4	0.1	0.0	0.0	0.0	0.0
30/24-28	2844.1	AD	3.0	50.5	1.5	O	70-80	32.7	1.0	P	7.5	0.2	M	3.5	0.1	M	5.8	0.2	0.0	0.0	0.0	0.0
30/24-31	3190.3	AD	2.0	44.8	0.9	O	70-80	34.9	0.7	P	10.7	0.2	M	5.1	0.1	P	4.5	0.1	0.0	0.0	0.0	0.0
30/24-28	2794.7	CHB	3.3	TR	TR	-	-	22.0	0.7	P	58.7	1.9	M	15.8	0.5	M	3.6	0.1	0.0	0.0	0.0	0.0
30/24-05	2849.3	CHB	3.2	TR	TR	-	-	8.5	0.3	P	72.6	2.3	M	5.3	0.2	P	3.1	0.1	0.0	0.0	10.6	0.3

Facies: AD = aeolian dune; CHB- channel bar

A = Weight% relevant size fraction; B = Weight% bulk sample;

Mixed-layer Ordering: RI= Randomly Interstratified (R0); O = Ordered Interstratification (R1); LR = Long-range Ordering (R3);

Crystallinity: VW = Very Well Crystallised; W = Well Crystallised; M = Moderately Crystallised; P = Poorly Crystallised.

653

654 Fig 1

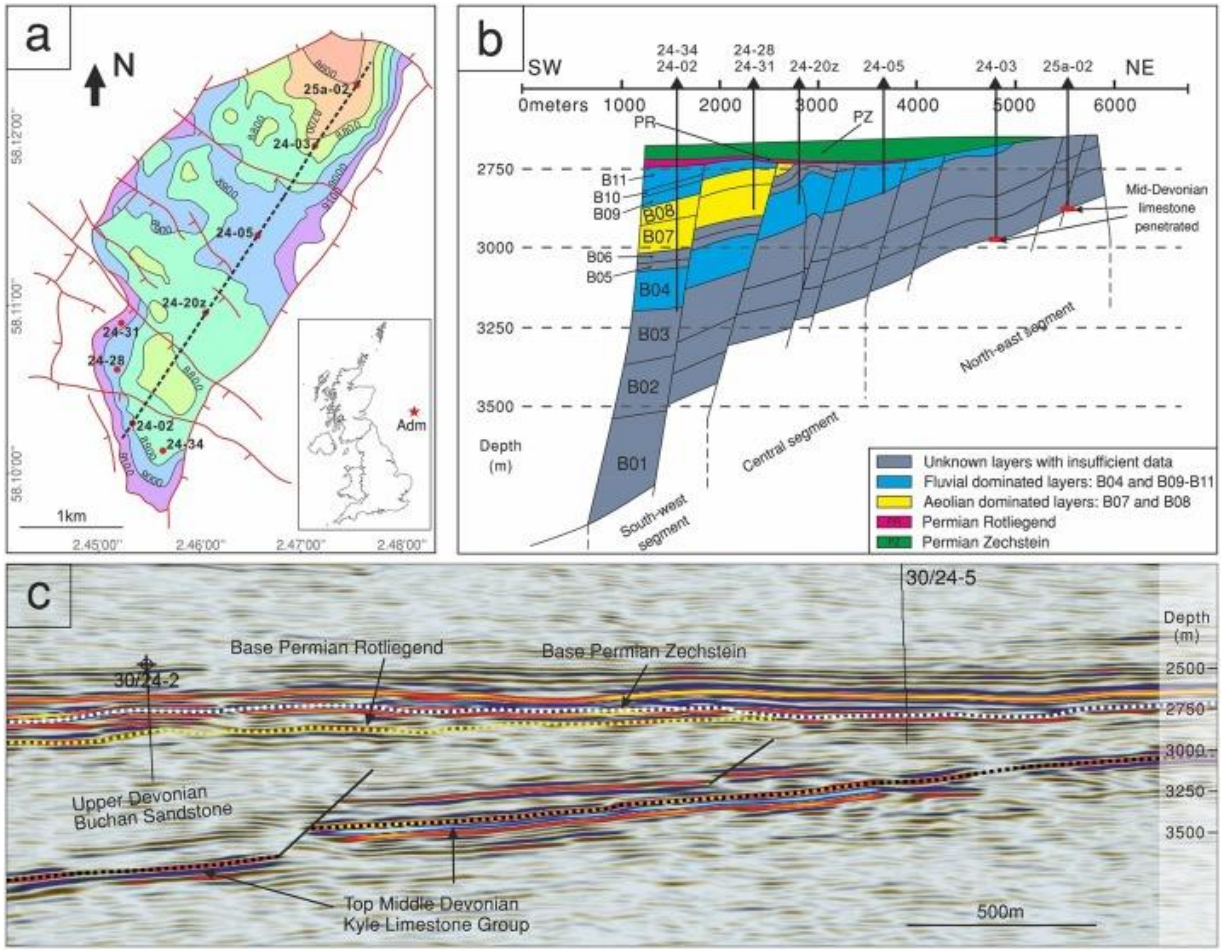
a
N
25a-02
24-03
24-05
24-20z
24-31
24-28
24-02
24-34
Adm
1km
58.12'00"
58.11'00"
58.10'00"
2.45'00"
2.46'00"
2.47'00"
2.48'00"
b
SW
NE
24-34
24-02
24-28
24-31
24-20z
24-05
24-03
25a-02
0meters
1000
2000
3000
4000
5000
6000
PR
PZ
2750
3000
3250
3500
Depth
(m)
B11
B10
B09
B08
B07
B06
B05
B04
B03
B02
B01
Mid-Devonian
limestone
penetrated
North-east segment
Central segment
South-west
segment
Unknown layers with insufficient data
Fluvial dominated layers: B04 and B09-B11
Aeolian dominated layers: B07 and B08
Permian Rotliegend
Permian Zechstein
c
30/24-5
30/24-2
Base Permian Rotliegend
Base Permian Zechstein
Upper Devonian
Buchan Sandstone
Top Middle Devonian
Kyle Limestone Group
500m
Depth
(m)
2500
2750
3000
3250
3500

Fig 2

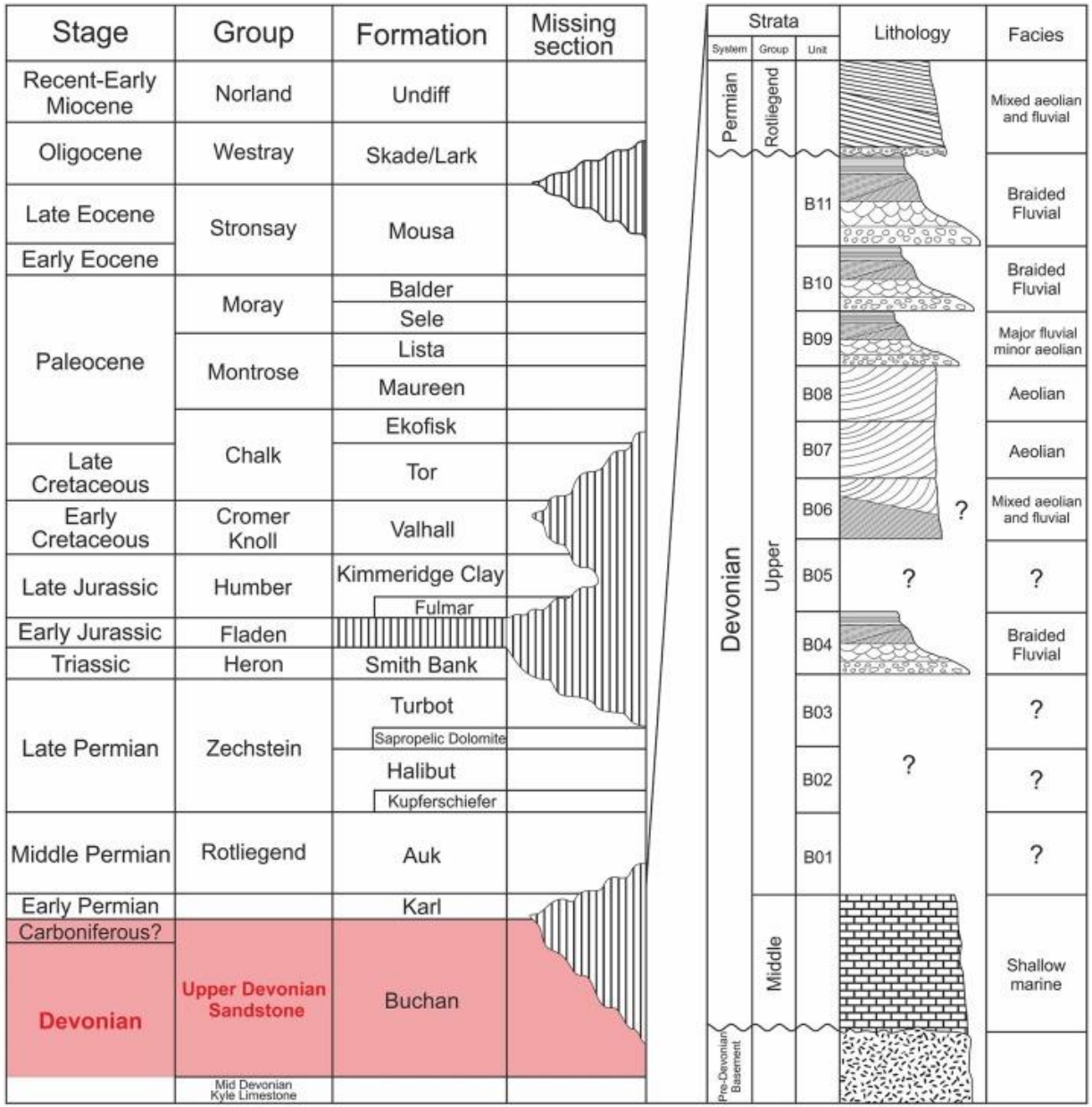
Stage
Group
Formation
Missing section
Recent-Early Miocene
Norland
Undiff
Oligocene
Westray
Skade/Lark
Late Eocene
Early Eocene
Stronsay
Mousa
Paleocene
Moray
Balder
Sele
Montrose
Lista
Maureen
Chalk
Ekofisk
Tor
Late Cretaceous
Early Cretaceous
Cromer Knoll
Valhall
Late Jurassic
Humber
Kimmeridge Clay
Fulmar
Early Jurassic
Fladen
Triassic
Heron
Smith Bank
Late Permian
Zechstein
Turbot
Sapropelic Dolomite
Halibut
Kupferschiefer
Middle Permian
Rotliegend
Auk
Early Permian
Karl
Carboniferous?
Devonian
Upper Devonian Sandstone
Buchan
Mid Devonian Kyle Limestone
Strata
System
Group
Unit
Lithology
Facies
Permian
Rotliegend
Devonian
Upper
Middle
Pre-Devonian Basement
B11
B10
B09
B08
B07
B06
B05
B04
B03
B02
B01
?
Mixed aeolian and fluvial
Braided Fluvial
Braided Fluvial
Major fluvial minor aeolian
Aeolian
Aeolian
Mixed aeolian and fluvial
?
Braided Fluvial
?
?
?
Shallow marine
Metamorphic or igneous basement
Conglomerates
Planar cross bedding sandstone
Inclined bedding sandstone with wind ripples
Limestone
Trough cross bedding sandstone
Silts or mudstone

658 Fig 3

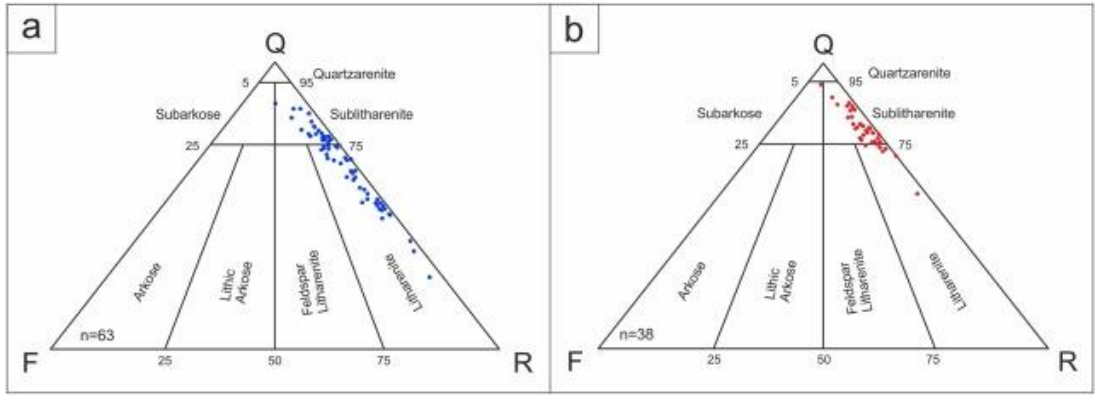

659

660 Fig 4

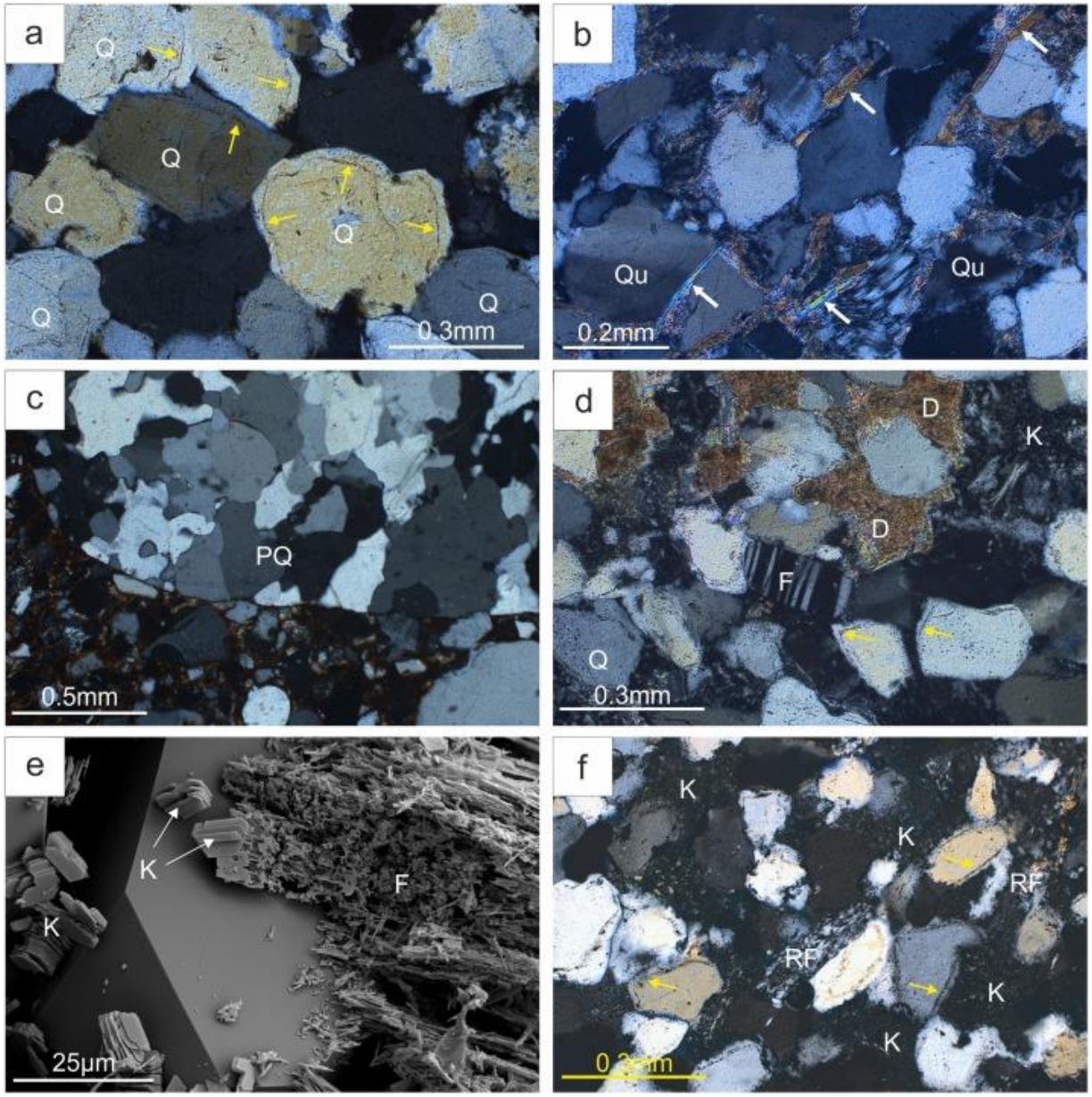
a
Q
Q
Q
Q
Q
Q
0.3mm
b
Qu
Qu
0.2mm
c
PQ
0.5mm
d
D
K
D
F
Q
0.3mm
e
K
K
F
25μm
f
K
K
RF
RF
K
K

661

662 Fig 5

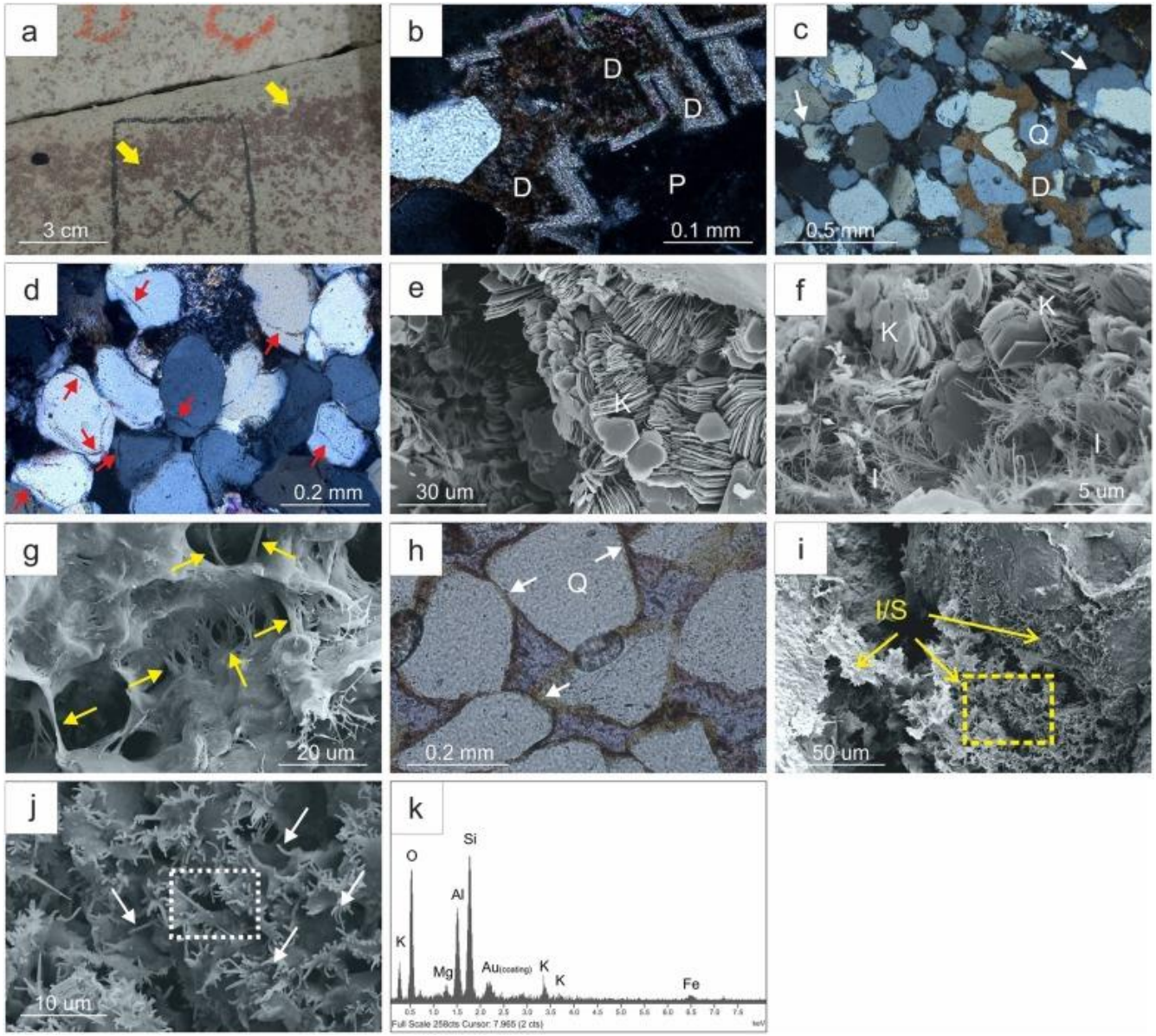
a
3 cm
b
D
D
D
P
0.1 mm
c
Q
D
0.5 mm
d
0.2 mm
e
K
30 um
f
K
K
I
I
5 um
g
20 um
h
Q
0.2 mm
i
I/S
50 um
j
10 um
k
O
Si
Al
K
Mg
Au(coating)
K
K
Fe
Full Scale 256cts Cursor: 7.965 (2 cts)

663

664 Fig 6

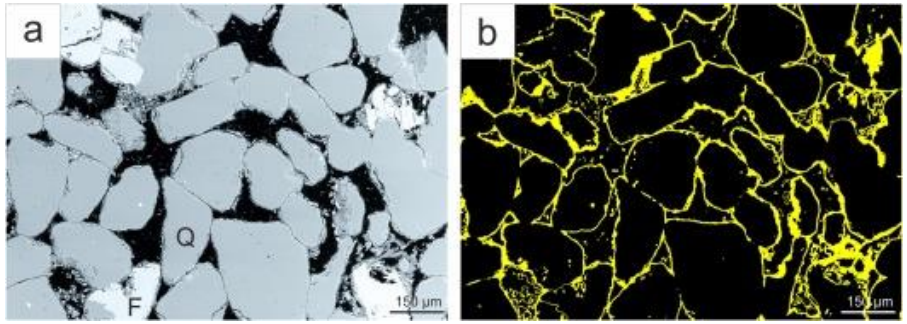

665

666 Fig 7

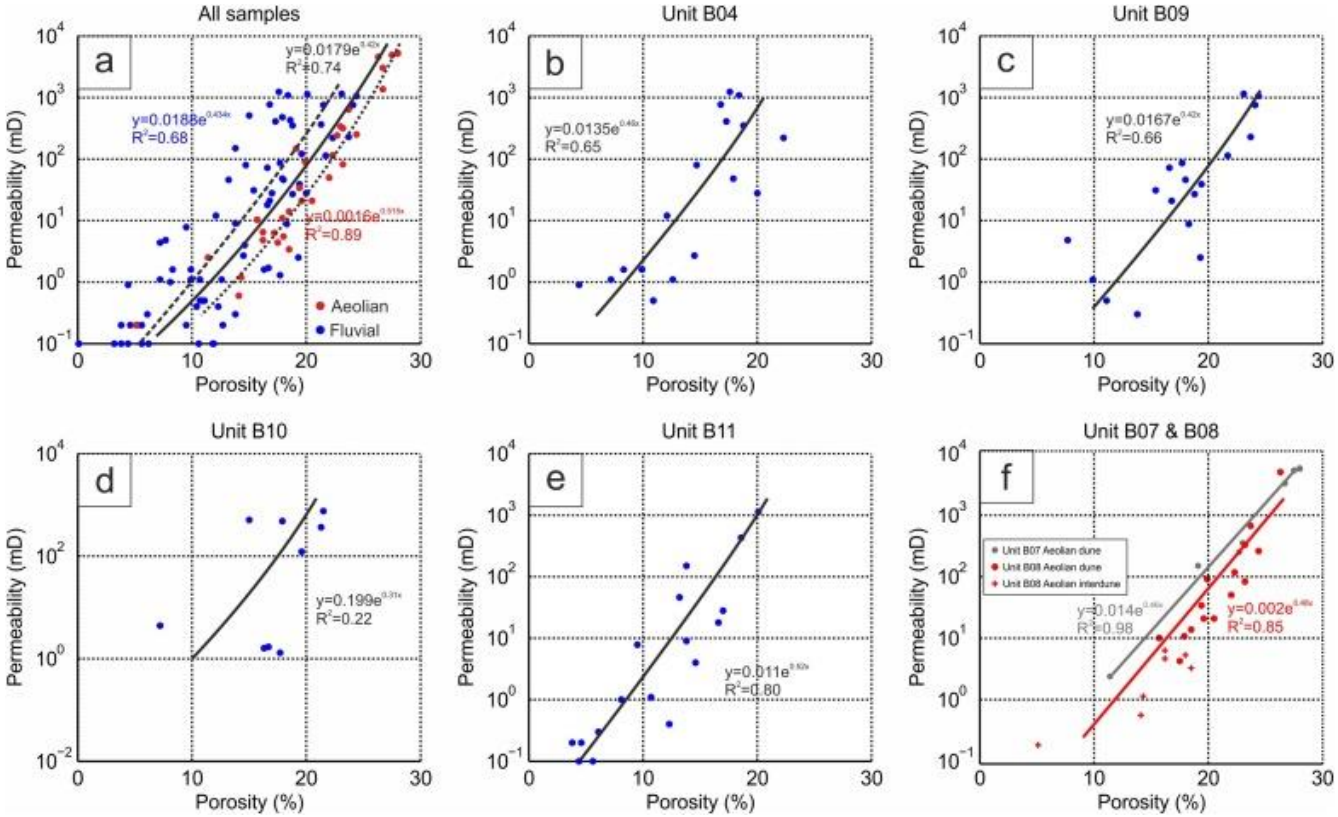
All samples
a
y=0.0179e^0.42x
R²=0.74
y=0.0188e^0.434x
R²=0.68
y=0.0016e^0.515x
R²=0.89
Aeolian
Fluvial
Unit B04
b
y=0.0135e^0.46x
R²=0.65
Unit B09
c
y=0.0167e^0.42x
R²=0.66
Unit B10
d
y=0.199e^0.37x
R²=0.22
Unit B11
e
y=0.011e^0.62x
R²=0.80
Unit B07 & B08
f
Unit B07 Aeolian dune
Unit B08 Aeolian dune
Unit B08 Aeolian interdune
y=0.014e^0.46x
R²=0.98
y=0.002e^0.48x
R²=0.85
Permeability (mD)
Porosity (%)

667

668 Fig 8

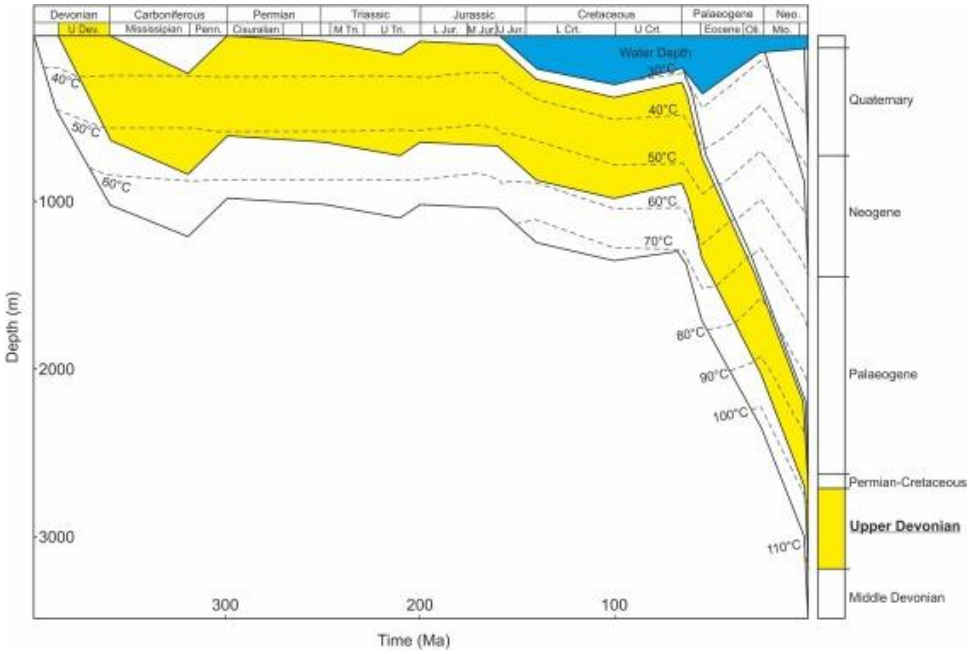
Devonian
Carboniferous
Permian
Triassic
Jurassic
Cretaceous
Palaeogene
Neo.
U Dev.
Mississipian
Penn.
Cisuralian
M Tri.
U Tri.
L Jur.
M Jur
U Jur.
L Crt.
U Crt.
Eocene
Olig.
Mio.
Water Depth
40°C
50°C
60°C
70°C
80°C
90°C
100°C
110°C
Depth (m)
1000
2000
3000
300
200
100
Time (Ma)
Quaternary
Neogene
Palaeogene
Permian-Cretaceous
Upper Devonian
Middle Devonian

669

670 Fig 9

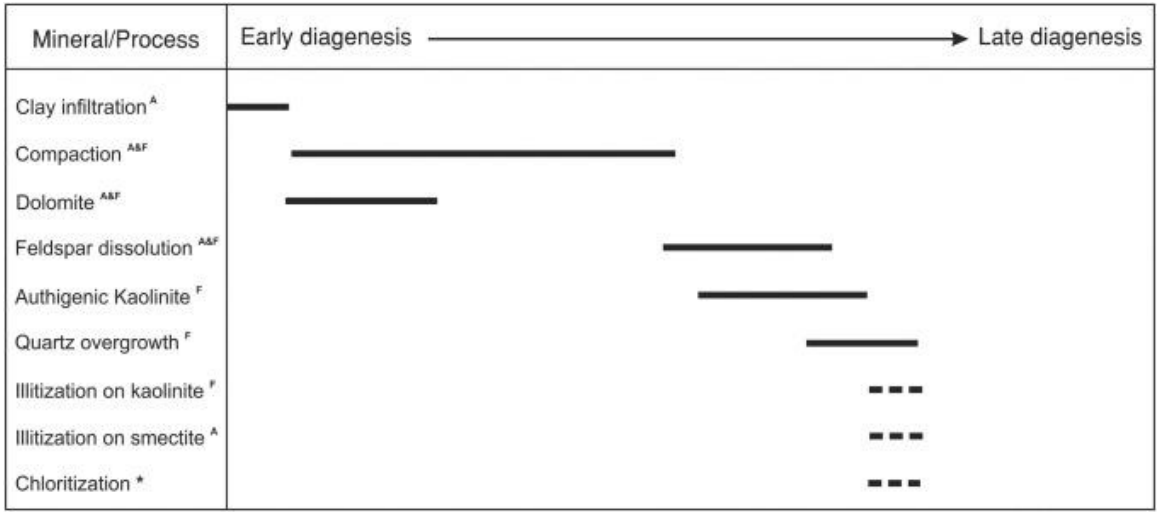

671

672 Fig 10

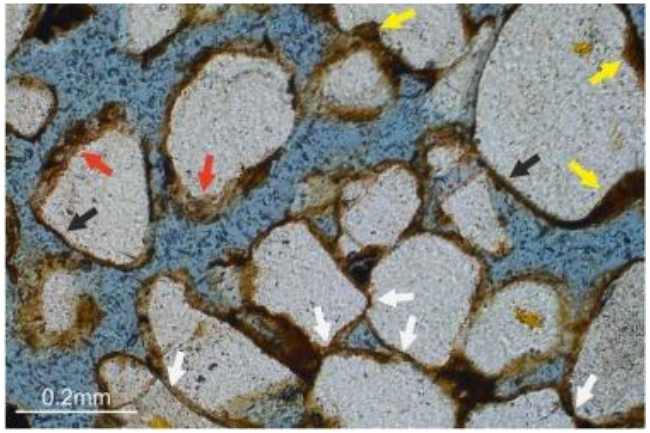

673

674 Fig 11

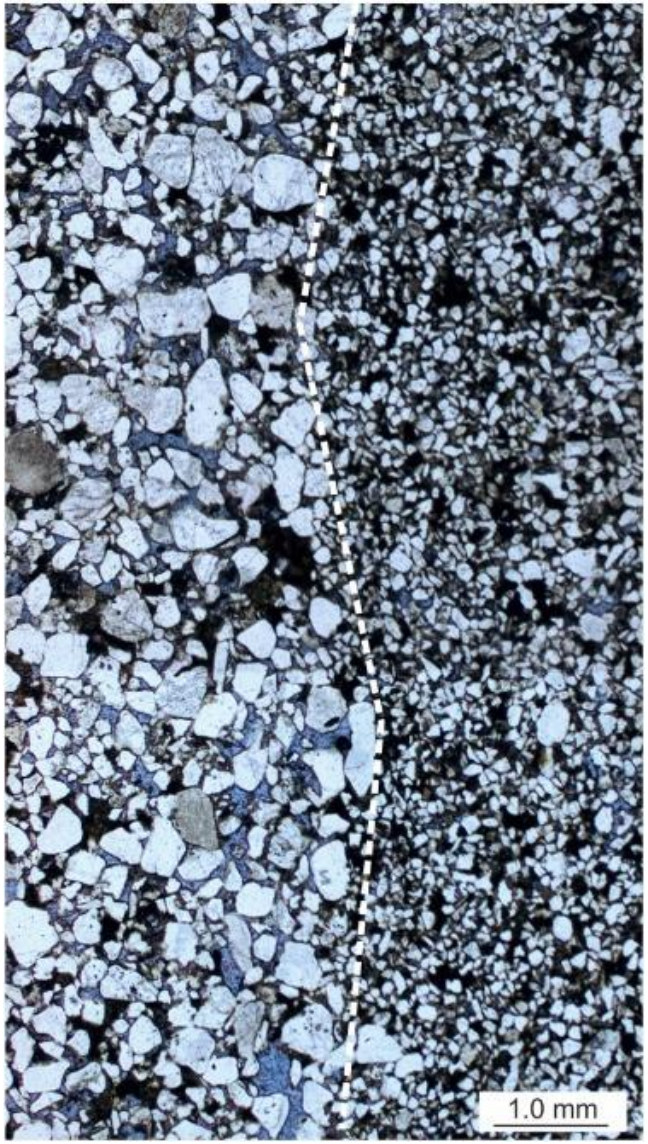

675

676 Fig 12

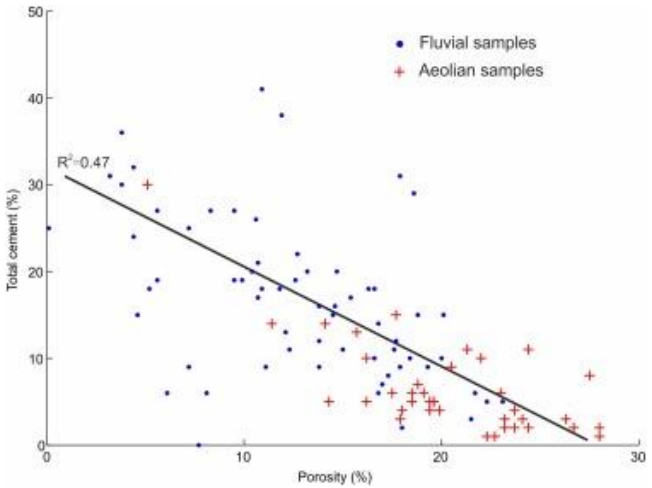

677

678 Fig 13

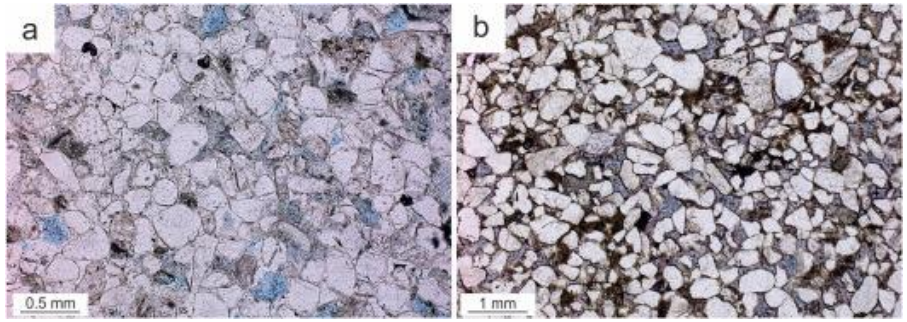

679

680 Fig 14

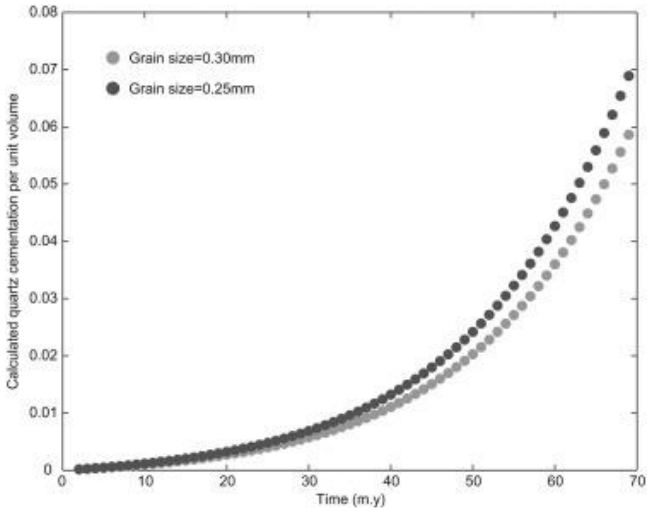
Grain size=0.30mm
Grain size=0.25mm
Calculated quartz cementation per unit volume
Time (m.y)
0.08
0.07
0.06
0.05
0.04
0.03
0.02
0.01
0
0
10
20
30
40
50
60
70

681